Acta Cryst E CRYSTALLOGRAPHIC COMMUNICATIONS

ISSN 2056-9890

(*N*,*N*′-Diisopropyldithiocarbamato)triphenyltin(IV): crystal structure, Hirshfeld surface analysis and computational study

Farah Natasha Haezam,[a] Normah Awang,[a]‡ Nurul Farahana Kamaludin,[a] Mukesh M. Jotani[b] and Edward R. T. Tiekink[c]*

[a]Environmental Health and Industrial Safety Programme, Faculty of Health Sciences, Universiti Kebangsaan Malaysia, Jalan Raja Muda Abdul Aziz, 50300 Kuala Lumpur, Malaysia, [b]Department of Physics, Bhavan's Sheth R. A. College of Science, Ahmedabad, Gujarat 380001, India, and [c]Research Centre for Crystalline Materials, School of Science and Technology, Sunway University, 47500 Bandar Sunway, Selangor Darul Ehsan, Malaysia. *Correspondence e-mail: edwardt@sunway.edu.my

Received 3 September 2019
Accepted 7 September 2019

Edited by W. T. A. Harrison, University of Aberdeen, Scotland

‡ Additional correspondence author, e-mail: awang_normah@yahoo.com.

Keywords: crystal structure; organotin; dithiocarbamate; Hirshfeld surface analysis; computational chemistry.

CCDC reference: 1952056

Supporting information: this article has supporting information at journals.iucr.org/e

The crystal and molecular structures of the title triorganotin dithiocarbamate, $[Sn(C_6H_5)_3(C_7H_{14}NS_2)]$, are described. The molecular geometry about the metal atom is highly distorted being based on a C_3S tetrahedron as the dithiocarbamate ligand is asymmetrically chelating to the tin centre. The close approach of the second thione-S atom [Sn···S = 2.9264 (4) Å] is largely responsible for the distortion. The molecular packing is almost devoid of directional interactions with only weak phenyl-C—H···C(phenyl) interactions, leading to centrosymmetric dimeric aggregates, being noted. An analysis of the calculated Hirshfeld surface points to the significance of H···H contacts, which contribute 66.6% of all contacts to the surface, with C···H/H···C [26.8%] and S···H/H···H [6.6%] contacts making up the balance.

1. Chemical context

Organotin(IV) compounds have long been investigated as potential anti-cancer agents (Gielen & Tiekink, 2005) and studies in this area continue. Further, organotin compounds have received much attention owing to their potential therapeutic potential as anti-fungal, anti-bacterial, anti-malarial and schizonticidal agents (Khan *et al.*, 2014). Metal dithiocarbamates have also encouraged much interest in the context of chemotherapeutic agents (Hogarth, 2012) and these include organotin(IV) dithiocarbamate compounds (Tiekink, 2008; Adeyemi & Onwudiwe, 2018). In view of the wide-range of applications/potential of organotin(IV) dithiocarbamate compounds and in continuation of on-going studies in this area (Khan *et al.*, 2015; Mohamad *et al.* 2016, 2017, 2018), the title compound, $Ph_3Sn[S_2CN(i\text{-}Pr)_2]$, (I), was synthesized and characterized spectroscopically. Herein, the crystal and molecular structures of (I) are described along with a detailed analysis of the molecular packing *via* the calculated Hirshfeld surfaces and computational chemistry study.

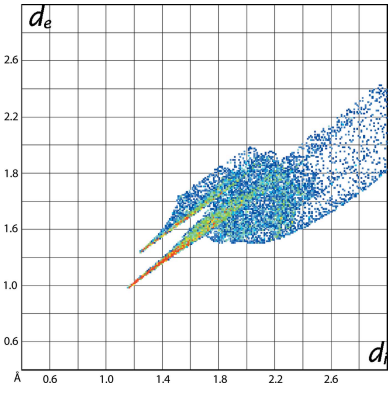

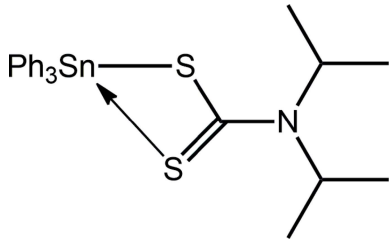

Table 1
Selected bond lengths (Å).

Sn—S1	2.4792 (4)	C1—S1	1.7587 (15)
Sn—S2	2.9264 (4)	C1—S2	1.7006 (16)
Sn—C11	2.1446 (14)	C1—N1	1.336 (2)
Sn—C21	2.1349 (15)	C5—N1	1.495 (2)
Sn—C31	2.1754 (15)	C2—N1	1.497 (2)

2. Structural commentary

The tin atom in (I), Fig. 1, is coordinated by an asymmetrically bound dithiocarbamate ligand and three *ipso*-carbon atoms of the phenyl groups (Table 1). The disparity in the Sn—S separations, *i.e.* Δ(Sn—S) = [(Sn—S$_l$) − (Sn—S$_s$)] = 0.45 Å (l = long, s = short), is rather great suggesting that the Sn···S2 interaction is weak. This is supported in the pattern of C—S bond lengths with that involving the more tightly bound S1 atom being nearly 0.06 Å longer than the equivalent bond with the weakly bound S2 atom. Despite this, a clear influence of the S2 atom is noted on the Sn—C bond lengths with the Sn—C31 bond length being significantly longer than the other Sn—C bonds, Table 1. The S2—Sn—C31 bond angle is 158.41 (4)° and is suggestive of a *trans*-influence exerted by the S2 atom; there is no other *trans* angle about the tin atom. If the coordination geometry is considered as tetrahedral, the range of tetrahedral angles is 93.24 (4)°, for S1—Sn—C31, to 119.87 (6)°, for C11—Sn—C21. The range of angles assuming a five-coordinate, C_3S_2, geometry is 65.260 (11)°, for the S1—Sn—S2 chelate angle to the aforementioned 158.41 (4)°. A descriptor for assigning coordination geometries to five-coordinate species is τ (Addison *et al.*, 1984). In the case of (I), this computes to 0.64, which indicates a geometry somewhat closer to an ideal trigonal bipyramid (τ = 1.0) than to an ideal square pyramid (τ = 0.0). Also included in Table 1 are the C—N bond lengths, which show C1—N1 to be significantly shorter than the C2—N1 and C5—N1 bond lengths, an observation consistent with a significant contribution of the $^{2-}S_2C{=}N^+(i\text{-}Pr)_2$ canonical form to the overall electronic structure of the dithiocarbamate ligand.

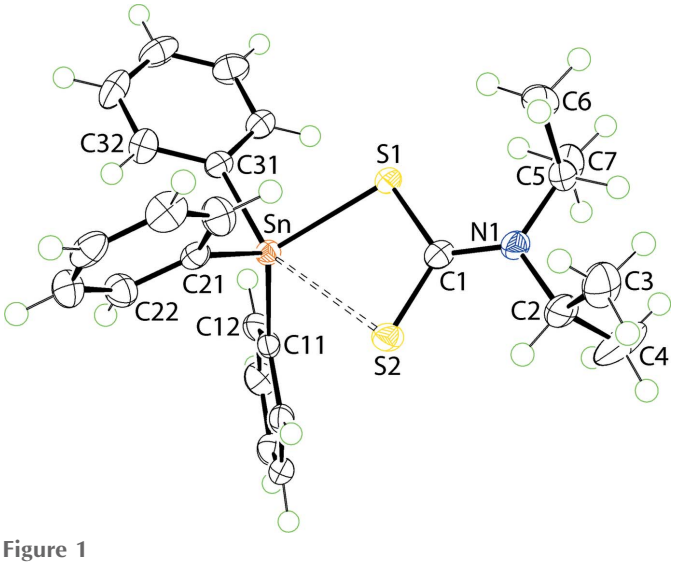

Figure 1
The molecular structure of (I) showing the atom-labelling scheme and displacement ellipsoids at the 70% probability level. The long Sn1···S2 contact is indicated by a double-dashed line.

Table 2
Hydrogen-bond geometry (Å, °).

D—H···*A*	*D*—H	H···*A*	*D*···*A*	*D*—H···*A*
C34—H34···C24^{i}	0.95	2.82	3.757 (3)	171

Symmetry code: (i) $-x+1, -y, -z$.

3. Supramolecular features

The geometric parameters characterizing the identified intermolecular interaction operating in the crystal of (I) are collated in Table 2. A phenyl-C—H···C(phenyl) contact less than the sum of the sum of the Waals radii (Spek, 2009) is noted to occur between centrosymmetrically related molecules, Fig. 2(*a*). This is an example of a localized C—H···π contact whereby the hydrogen atom directed towards a single carbon atom of the ring as opposed to a delocalized interaction where the hydrogen atom (or halide atom or lone-pair of electrons) is directed towards the centroid of the ring (Schollmeyer *et al.*, 2008; Tiekink, 2017).

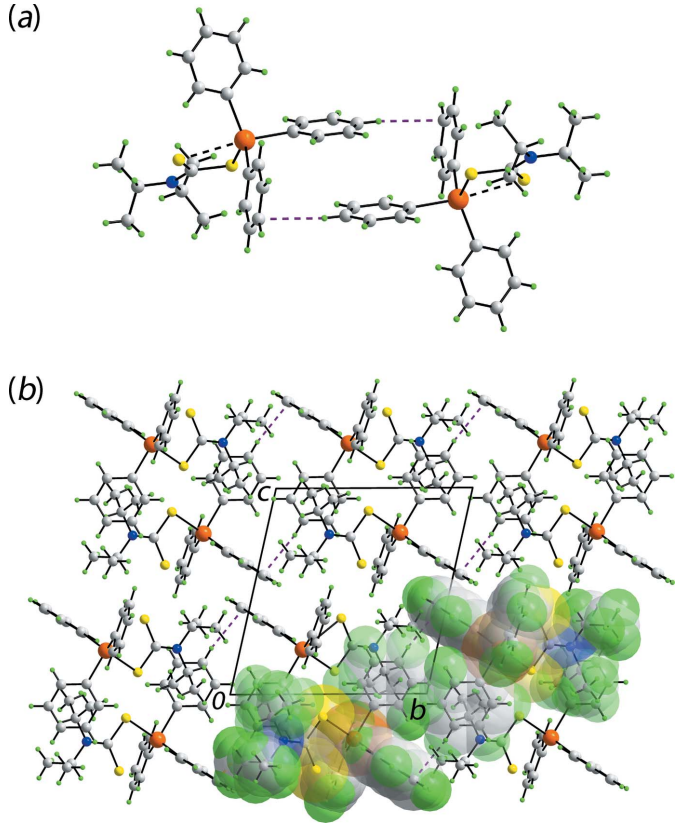

Figure 2
Molecular packing in the crystal of (I): (*a*) supramolecular dimer sustained by localized phenyl-C—H···C(phenyl) interactions shown as purple dashed lines and (*b*) a view of the unit-cell contents in projection down the *a* axis. One column of dimeric aggregates is highlighted in space-filling mode.

Table 3
Summary of short interatomic contacts (Å) in (I).

The interatomic distances are calculated in *Crystal Explorer 17* (Turner *et al.*, 2017) whereby the *X*—H bond lengths are adjusted to their neutron values.

Contact	Distance	Symmetry operation
H7*A*···H12	2.09	$1-x, 1-y, -z$
H13···H26	2.26	$1+x, y, z$
C12···H36	2.65	$1-x, 1-y, -z$
C13···H26	2.68	$1+x, y, z$
C16···H23	2.65	$1-x, -y, 1-z$
C24···H34	2.68	$1-x, -y-z$

4. Hirshfeld surface analysis

The Hirshfeld surface calculations for (I) were performed employing *Crystal Explorer 17* (Turner *et al.*, 2017) and recently published protocols (Tan *et al.*, 2019). In the absence of classical hydrogen bonds, the influence of the localized C—H···π interaction, Table 2, as well as interatomic H···H and C···H/H···C contacts, Table 3, upon the molecular packing are evident as the diminutive-red spots near the participating carbon and hydrogen atoms on the Hirshfeld surfaces mapped over d_{norm} in Fig. 3. It is also noted that with the exception of the methyl-H7*A* atom, all of the specified interatomic contacts only involve the carbon and hydrogen atoms of the coordinated phenyl rings, Table 3. On the Hirshfeld surface mapped over electrostatic potential in Fig. 4, the light-blue and faint-red regions, corresponding to positive and negative electrostatic potential, respectively, occur about the di-*iso*-propyl and triphenyltin groups, respectively.

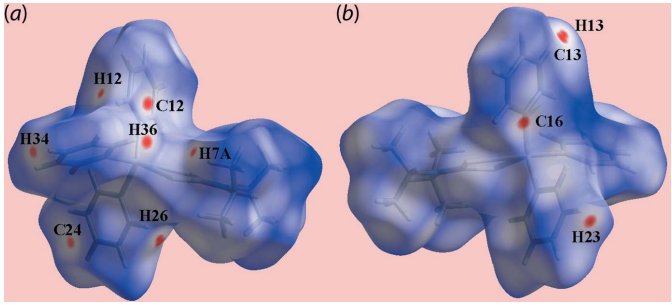

Figure 3
Two views of Hirshfeld surface for (I) mapped over d_{norm} in the range −0.085 to +1.355 (arbitrary units), highlighting short interatomic H···H and C···H/H···C contacts as diminutive red spots near the respective atoms.

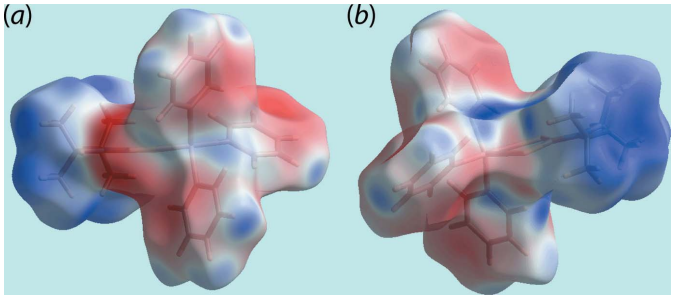

Figure 4
Two views of Hirshfeld surface mapped over the electrostatic potential (the red and blue regions represent negative and positive electrostatic potentials, respectively) in the range −0.032 to +0.035 atomic units.

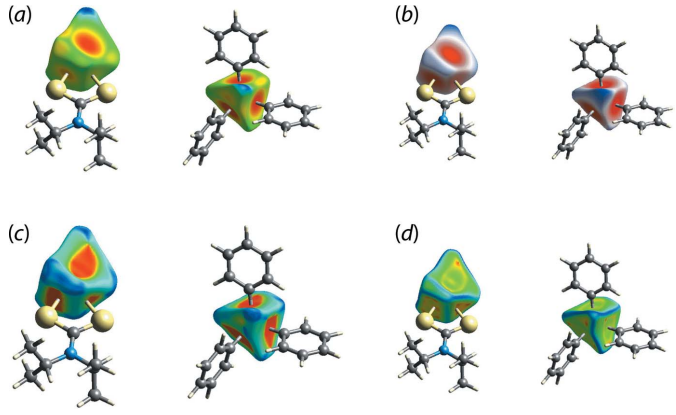

Figure 5
The Hirshfeld surfaces of the tin centre in (I) highlighting the coordination by the dithiocarbamate ligand (left-hand images) and the phenyl rings (right-hand images) mapped over (*a*) the distance, d_e, external to the surface in the range −0.981 to 2.436 Å, (*b*) d_{norm} in the range −0.890 to +1.135 Å, (*c*) the shape-index (S) from −1.0 to +1.0 (arbitrary units) and (*d*) curvedness (C) from −4.0 to +0.4 (arbitrary units).

As reported recently (Pinto *et al.*, 2019), in addition to analysing the nature and strength of intermolecular interactions among molecules, the analyses of Hirshfeld surfaces can also provide useful insight into metal–ligand/donor atom interactions in coordination compounds. Thus, the distance from the surface to the nearest external (d_e) and internal (d_i) nuclei, the shape-index (S) and the curvedness (C) can also be plotted. Accordingly, Fig. 5 illustrates the Hirshfeld surfaces for the tin atom coordinated by dithiocarbamate ligand as well as by the three phenyl groups. The close proximity of the dithiocarbamate-S1 and phenyl-C11, C21 and C31 atoms to the tin centre are characterized as bright-red regions perpendicular to bond directions on the Hirshfeld surfaces mapped over d_e, Fig. 5(*a*), and d_{norm}, Fig. 5(*b*), whereas the comparatively weak Sn—S2 interaction appears as the faint-red region. The longer Sn—C31 bond compared to other two Sn—C bonds, Table 1, is also characterized from these Hirshfeld surfaces through the curvature of the red region. The Sn—S1 and Sn—C bonds result in the large red regions on the shape-index mapping in Fig. 5(*c*) compared to a small red region for the Sn—S2 bond. On the Hirshfeld surfaces mapped over curvedness in Fig. 5(*d*), the strength of the tin–ligand bonds are characterized as the yellow areas separated by green regions. The coordination bonds for tin are also rationalized in the fingerprint plot taking into account only the Hirshfeld surface about the metal atom, Fig. 6. The distribution of green points having upper short spike at $d_e + d_i \sim 2.4$ Å and the lower, long red spike at $d_e + d_i \sim 2.1$ Å are the result of the Sn—S and Sn—C bonds, respectively. This asymmetric distribution of points about the diagonal lacking homogeneity in colouration is due to the distorted coordination geometry about the tin atom.

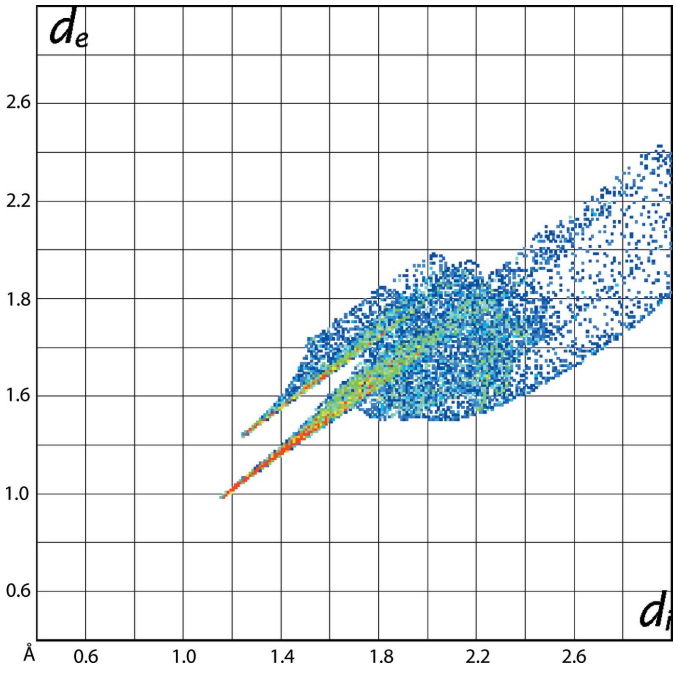

Figure 6
The fingerprint plot taking into account only the Hirshfeld surface about the tin atom.

It is clear from the the calculation of the overall two-dimensional fingerprint plot for (I), Fig. 7(*a*), that the plot is asymmetric about the (d_e, d_i) diagonal in the longer distance regions and have contributions only from the interatomic contacts involving carbon, hydrogen and sulfur atoms, Table 4. The two-dimensional fingerprint plots delineated into H···H, C···H/H···C, C···C and S···H/H···S contacts are shown in Fig. 7(*b*)–(*d*), respectively. In the fingerprint plot delineated into H···H contacts in Fig. 7(*b*), the presence of the short interatomic H···H interaction involving the methyl-H7*A* and phenyl-H12 atoms is evident as the pair of short overlapping peaks at $d_e + d_i \sim 2.1$ Å with the other short interatomic H···H contact (Table 3) merged within the plot. The intermolecular C—H···C interactions describing the localized C—H···π contacts are evidenced by a pronounced pair of characteristic wings around (d_e, d_i) ~(1.2 Å, 1.8Å) and ~(1.8 Å, 1.2 Å) in

Table 4
Percentage contributions of interatomic contacts to the Hirshfeld surface for (I).

Contact	Percentage contribution
H···H	66.5
C···H/H···C	26.8
S···H/H···S	6.6
C···S/S···C	0.1

Table 5
Summary of interaction energies (kJ mol^{-1}) calculated for (I).

Contact	R (Å)	E_{ele}	E_{pol}	E_{dis}	E_{rep}	E_{tot}
H7*A*···H12^{i} +	6.30					
H36···C12^{i}		−17.5	−7.0	−112.7	68.0	−68.8
H13···H26^{ii} +	9.76					
C13···H26^{ii}		−8.7	−2.0	−31.6	18.0	−24.0
C16···H23^{iii}	9.46	−12.9	−2.0	−41.9	29.5	−28.2
C24···H34^{iv}	10.62	−11.0	−2.8	−33.8	21.6	−26.0

Notes: Symmetry operations: (i) $1-x, 1-y, -z$; (ii) $1+x, y, z$; (iii) $1-x, -y, 1-z$; (iv) $1-x, -y, -z$.

the fingerprint plot delineated into C···H/H···C contacts shown in Fig. 7(*c*). The other short interatomic C···H contacts summarized in Table 3 appear as the pair of forceps-like tips at $d_e + d_i \sim 2.7$ Å. The fingerprint plot delineated into S···H/H···S contacts in Fig. 7(*d*) indicate that sulfur atoms are nearly at van der Waals separation from the symmetry-related hydrogen atoms.

5. Computational chemistry

The pairwise interaction energies between the molecules within the crystal were calculated using *Crystal Explorer 17* (Turner *et al.*, 2017) and summing up the four energy components: electrostatic (E_{ele}), polarization (E_{pol}), dispersion (E_{dis}) and exchange-repulsion (E_{rep}). The energies were obtained using the wave function calculated at the HF/STO-3G level of theory. The strength and the nature of intermolecular interactions in terms of their energies are summarized in Table 5. An analysis of these reveals that the dispersion energy component makes the greatest contribution

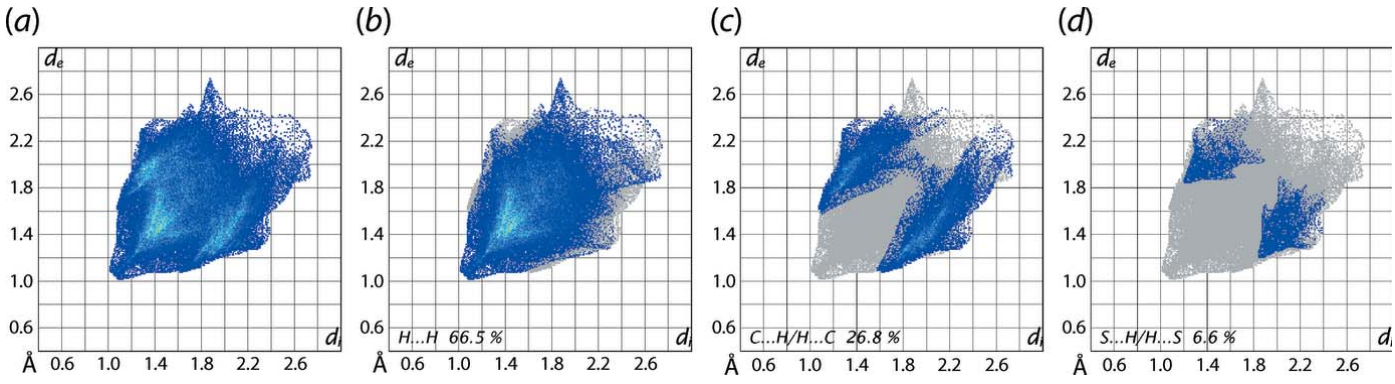

Figure 7
(*a*) A comparison of the full two-dimensional fingerprint plot for (I) and those delineated into (*b*) H···H, (*c*) C···H/H···C and (*d*) S···H/H···S contacts.

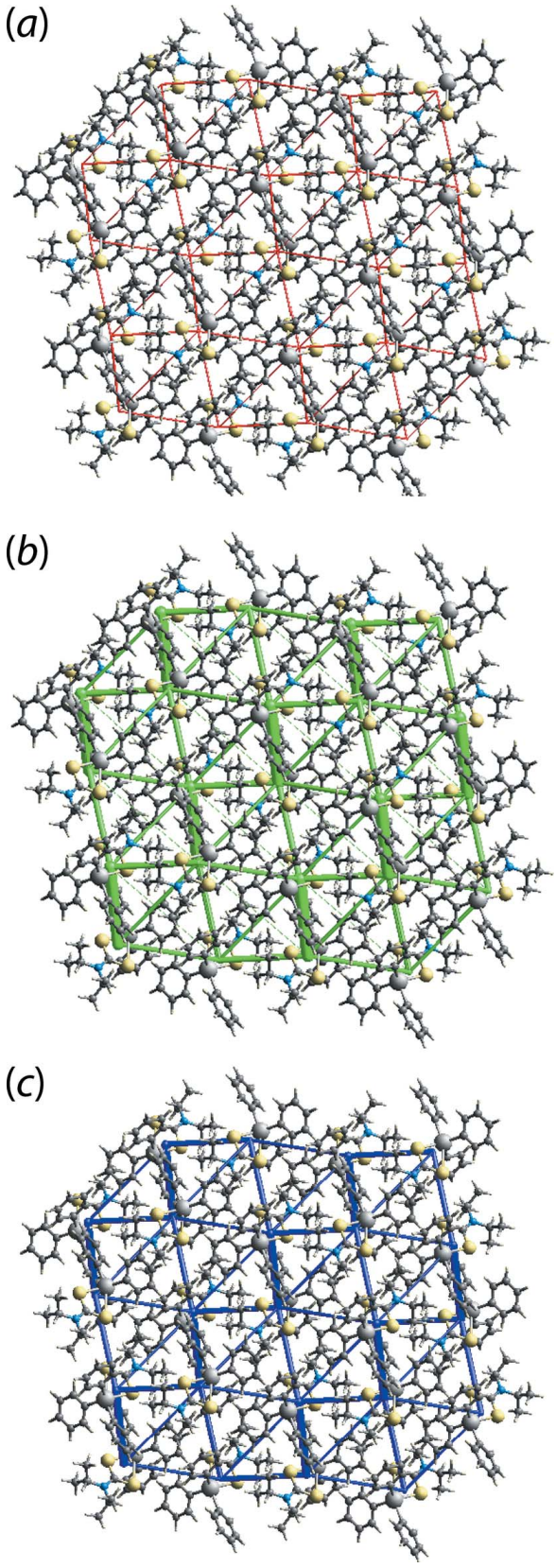

Figure 8
The energy frameworks calculated for (I) viewed down the *c*-axis direction showing the (*a*) electrostatic potential force, (*b*) dispersion force and (*c*) total energy. The energy frameworks were adjusted to the same scale factor of 30 with a cut-off value of 3 kJ mol^{-1} within 2 × 2 × 2 unit cells.

to the energies in the absence of classical hydrogen (electrostatic) bonds. Among the short interatomic contacts listed in Table 5, the intermolecular phenyl-C—H36···C12 contact combined with the methyl-H7*A*···H12(phenyl) interaction, occurring between the same pair of symmetry-related molecules, gives rise to the maximum total energy of interaction, compared to the other interactions, which have almost the same energy values.

The graphical representation of the magnitudes of intermolecular energies in Fig. 8, *i.e.* energy frameworks, relies on a red, green and blue colour code scheme, reflecting the E_{ele}, E_{disp} and E_{tot} components, respectively. For the direct comparison of magnitudes of interaction energies, their magnitudes were adjusted to same scale factor of 30 with a cut-off value of 3 kJ mol^{-1} within 2 × 2 × 2 unit cells. It is clear from Fig. 8 that the green cylinders joining the centroids of molecular pairs highlighting the dispersion components make a significant contribution to the supramolecular architecture in the crystal.

6. Database survey

As indicated in a recent report (Mohamad *et al.*, 2018), there are nearly 50 crystal structures available for molecules of the general formula $Ph_3Sn(S_2CNRR')$ and, with a number of these having multiple molecules in the asymmetric unit, there are almost 60 independent molecules. These conform to the same structural motif. An analysis of the key geometric parameters defining the mode of coordination of the dithiocarbamate ligands showed that there were no systematic variations that could be correlated with the nature of the dithiocarbamate ligand, *i.e.* *R*/*R*′ substituents. This observation is borne out by DFT calculations on different organotin systems that proved the influence of molecular packing on (non-systematic) geometric parameters, including metal–sulfur/halide bonds (Buntine *et al.*, 1998*a*,*b*, 1999). In terms of $Ph_3Sn(S_2CNRR')$, the mean Sn—S_s bond length is 2.47 Å (standard deviation = 0.013 Å) and the average Sn—S_l bond length is 3.04 Å (0.070 Å). The Sn—S_s and Sn—S_l bond lengths in (I) both fall within 2σ of their respective means.

The homogeneity in the molecular structures of $Ph_3Sn(S_2CNRR')$ is quite remarkable. Structural diversity is well-established for the organotin dithiocarbamates (Tiekink, 2008; Muthalib *et al.*, 2014) such as for molecules of the general formula $R''_2Sn(S_2CNRR')_2$, for which four distinct structural motifs are known (Zaldi *et al.*, 2017). Also, the behaviour of triphenyltin dithiocarbamates contrasts the analogous chemistry of triphenyltin carboxylates (Tiekink, 1991). These are often monomeric (*e.g.* Basu Baul *et al.*, 2001), as for (I), but, polymeric examples are known (*e.g.* Willem *et al.*, 1997; Smyth & Tiekink, 2000). The polymeric structures occur when the carboxylate ligands are bidentate bridging, leading to *trans*-C_3O_2 trigonal–bipyramidal coordination geometries for the tin atoms. This fundamental difference in structural chemistry arises as a result of the significant contribution of the $^{2-}S_2C{=}N^+RR'$ canonical form to the electronic structure of the dithiocarbamate anion, as discussed

Table 6
Experimental details.

Crystal data	
Chemical formula	$[Sn(C_6H_5)_3(C_7H_{14}NS_2)]$
M_r	526.30
Crystal system, space group	Triclinic, $P\overline{1}$
Temperature (K)	100
a, b, c (Å)	9.7572 (1), 11.7030 (2), 11.7602 (2)
α, β, γ (°)	74.419 (1), 80.114 (1), 67.285 (2)
V (Å^3)	1189.71 (4)
Z	2
Radiation type	Cu $K\alpha$
μ (mm^{-1})	10.25
Crystal size (mm)	0.12 × 0.11 × 0.08
Data collection	
Diffractometer	Rigaku XtaLAB Synergy Dualflex AtlasS2
Absorption correction	Gaussian (*CrysAlis PRO*; Rigaku OD, 2018)
T_{min}, T_{max}	0.840, 1.000
No. of measured, independent and observed [$I > 2\sigma(I)$] reflections	28219, 4248, 4231
R_{int}	0.022
(sin $\theta/\lambda)_{max}$ (Å^{-1})	0.597
Refinement	
$R[F^2 > 2\sigma(F^2)]$, $wR(F^2)$, S	0.015, 0.040, 1.00
No. of reflections	4248
No. of parameters	266
H-atom treatment	H-atom parameters constrained
$\Delta\rho_{max}$, $\Delta\rho_{min}$ (e Å^{-3})	0.36, −0.44

Computer programs: *CrysAlis PRO* (Rigaku OD, 2018), *SHELXS* (Sheldrick, 2015*a*), *SHELXL2014* (Sheldrick, 2015*b*), *ORTEP-3 for Windows* (Farrugia, 2012), *DIAMOND* (Brandenburg, 2006) and *publCIF* (Westrip, 2010).

above. The formal negative charge on each sulfur atom makes this ligand a very efficient chelator which effectively reduces the Lewis acidity of the tin centre. Far from being a curiosity, such behaviour, *i.e.* dithiocarbamate ligands reducing the Lewis acidity of metal centres, when compared to related xanthate (^-S_2COR) and dithiophopshate [$(^-S_2P(OR)_2$] ligands, leads to stark differences in coordination propensities in zinc-triad element 1,1-dithiolate compounds, as has been reviewed recently (Tiekink, 2018*a*,*b*).

7. Synthesis and crystallization

All chemicals and solvents were used as purchased without purification. The melting point was determined using an automated melting point apparatus (MPA 120 EZ-Melt). Carbon, hydrogen, nitrogen and sulfur analyses were performed on a Leco CHNS-932 Elemental Analyzer.

Di-*iso*-propylamine (Aldrich; 1.41 ml, 10 mmol) dissolved in ethanol (30 ml) was stirred under ice-bath conditions at 277 K for 20 mins. A 25% ammonia solution (1–2 ml) was added to provide basic conditions. Then, a cold ethanolic solution of carbon disulfide (0.60 ml, 10 mmol) was added dropwise into the solution followed by stirring for 2 h. After that, triphenyltin(IV) chloride (Merck; 3.85 g, 10 mmol) dissolved in ethanol (20–30 ml) was added dropwise into the solution followed by further stirring for 2 h. The precipitate that formed was filtered and washed a few times with cold ethanol to remove impurities. Finally, the colourless precipitate was dried in a desiccator. Recrystallization was carried out by dissolving the compound in a chloroform and ethanol mixture (1:1 *v*/*v*). This solution was allowed to slowly evaporate at room temperature yielding colourless slabs of (I). Yield: 47%, m. p.: 437.8–440.2 K. Elemental analysis: Calculated (%): C 57.07, H 5.51, N 2.66, S 12.19. Found (%): C 57.39, H 5.31, N 2.48, S 11.26.

8. Refinement

Crystal data, data collection and structure refinement details are summarized in Table 6. Carbon-bound H atoms were placed in calculated positions (C—H = 0.95–1.00 Å) and were included in the refinement in the riding model approximation, with U_{iso}(H) set to 1.2–1.5U_{eq}(C).

Acknowledgements

We gratefully acknowledge the Faculty of Health Sciences and the Faculty of Science and Technology of the Universiti Kebangsaan Malaysia for providing essential laboratory facilities and for technical support from the laboratory assistants. The Universiti Malaysia Terengganu is thanked for the elemental analysis. The authors also thank the Research Centre of Crystalline Materials X-ray crystallography laboratory for the X-ray intensity data.

Funding information

This work was supported by the Fundamental Research Grant Scheme (FRGS/1/2018/STG01/UKM/02/20) awarded by the Ministry of Education (MOE). Crystallographic research at Sunway University is supported by Sunway University Sdn Bhd (grant No. STR-RCTR-RCCM-001-2019).

References

Addison, A. W., Rao, T. N., Reedijk, J., van Rijn, J. & Verschoor, G. C. (1984). *J. Chem. Soc. Dalton Trans.* pp. 1349–1356.
Adeyemi, J. O. & Onwudiwe, D. C. (2018). *Molecules*, **23** article No. 2571.
Basu Baul, T. S., Dhar, S., Pyke, S. M., Tiekink, E. R. T., Rivarola, E., Butcher, R. & Smith, F. E. (2001). *J. Organomet. Chem.* **633**, 7–17.
Brandenburg, K. (2006). *DIAMOND*. Crystal Impact GbR, Bonn, Germany.
Buntine, M. A., Hall, V. J., Kosovel, F. J. & Tiekink, E. R. T. (1998*a*). *J. Phys. Chem. A*, **102**, 2472–2482.
Buntine, M. A., Hall, V. J. & Tiekink, E. R. T. (1998*b*). *Z. Kristallogr.* **213**, 669–678.
Buntine, M. A., Hall, V. J. & Tiekink, E. R. T. (1999). *Z. Kristallogr.* **214**, 124–134.
Farrugia, L. J. (2012). *J. Appl. Cryst.* **45**, 849–854.
Gielen, M. & Tiekink, E. R. T. (2005). *Metallotherapeutic drugs and metal-based diagnostic agents: the use of metals in medicine*, edited by M. Gielen & E. R. T. Tiekink, pp. 421–439. Chichester: John Wiley & Sons Ltd.
Hogarth, G. (2012). *Mini Rev. Med. Chem.* **12**, 1202–1215.
Khan, N., Farina, Y., Mun, L. K., Rajab, N. F. & Awang, N. (2014). *J. Mol. Struct.* **1076**, 403–410.
Khan, N., Farina, Y., Mun, L. K., Rajab, N. F. & Awang, N. (2015). *Polyhedron*, **85**, 754–760.

Mohamad, R., Awang, N., Kamaludin, N. F. & Abu Bakar, N. F. (2016). *Res. J. Pharm. Biol. Chem. Sci.* **7**, 1269–1274.
Mohamad, R., Awang, N., Kamaludin, N. F., Jotani, M. M. & Tiekink, E. R. T. (2017). *Acta Cryst.* E**73**, 260–265.
Mohamad, R., Awang, N., Kamaludin, N. F., Jotani, M. M. & Tiekink, E. R. T. (2018). *Acta Cryst.* E**74**, 630–637.
Muthalib, A. F. A., Baba, I., Khaledi, H., Ali, H. M. & Tiekink, E. R. T. (2014). *Z. Kristallogr.* **229**, 39–46.
Pinto, C. B., Dos Santos, L. H. R. & Rodrigues, B. L. (2019). *Acta Cryst.* C**75**, 707–716.
Rigaku OD (2018). *CrysAlis PRO*. Rigaku Oxford Diffraction Corporation, Yarnton, England.
Schollmeyer, D., Shishkin, O. V., Rühl, T. & Vysotsky, M. O. (2008). *CrystEngComm*, **10**, 715–723.
Sheldrick, G. M. (2015*a*). *Acta Cryst.* A**71**, 3–8.
Sheldrick, G. M. (2015*b*). *Acta Cryst.* C**71**, 3–8.
Smyth, D. R. & Tiekink, E. R. T. (2000). *Z. Kristallogr. New Cryst. Struct.* **215**, 81–82.
Spek, A. L. (2009). *Acta Cryst.* D**65**, 148–155.
Tan, S. L., Jotani, M. M. & Tiekink, E. R. T. (2019). *Acta Cryst.* E**75**, 308–318.
Tiekink, E. R. T. (1991). *Appl. Organomet. Chem.* **5**, 1–23.
Tiekink, E. R. T. (2008). *Appl. Organomet. Chem.* **22**, 533–550.
Tiekink, E. R. T. (2017). *Coord. Chem. Rev.* **345**, 209–228.
Tiekink, E. R. T. (2018*a*). *Crystals*, **8**, article no. 292.
Tiekink, E. R. T. (2018*b*). *Crystals*, **8**, article no. 18.
Turner, M. J., Mckinnon, J. J., Wolff, S. K., Grimwood, D. J., Spackman, P. R., Jayatilaka, D. & Spackman, M. A. (2017). Crystal Explorer 17. The University of Western Australia.
Westrip, S. P. (2010). *J. Appl. Cryst.* **43**, 920–925.
Willem, R., Bouhdid, A., Mahieu, B., Ghys, L., Biesemans, M., Tiekink, E. R. T., de Vos, D. & Gielen, M. (1997). *J. Organomet. Chem.* **531**, 151–158.
Zaldi, N. B., Hussen, R. S. D., Lee, S. M., Halcovitch, N. R., Jotani, M. M. & Tiekink, E. R. T. (2017). *Acta Cryst.* E**73**, 842–848.

supporting information

Acta Cryst. (2019). E**75**, 1479-1485 [https://doi.org/10.1107/S2056989019012490]

(*N*,*N*′-Diisopropyldithiocarbamato)triphenyltin(IV): crystal structure, Hirshfeld surface analysis and computational study

Farah Natasha Haezam, Normah Awang, Nurul Farahana Kamaludin, Mukesh M. Jotani and Edward R. T. Tiekink

Computing details

Data collection: *CrysAlis PRO* (Rigaku OD, 2018); cell refinement: *CrysAlis PRO* (Rigaku OD, 2018); data reduction: *CrysAlis PRO* (Rigaku OD, 2018); program(s) used to solve structure: *SHELXS* (Sheldrick, 2015*a*); program(s) used to refine structure: *SHELXL2014* (Sheldrick, 2015*b*); molecular graphics: *ORTEP-3 for Windows* (Farrugia, 2012) and *DIAMOND* (Brandenburg, 2006); software used to prepare material for publication: *publCIF* (Westrip, 2010).

(*N*,*N*′-Diisopropyldithiocarbamato)triphenyltin(IV)

Crystal data

$[Sn(C_6H_5)_3(C_7H_{14}NS_2)]$
M_r = 526.30
Triclinic, $P\overline{1}$
a = 9.7572 (1) Å
b = 11.7030 (2) Å
c = 11.7602 (2) Å
α = 74.419 (1)°
β = 80.114 (1)°
γ = 67.285 (2)°
V = 1189.71 (4) Å^3
Z = 2
$F(000)$ = 536
D_x = 1.469 Mg m^{-3}
Cu $K\alpha$ radiation, λ = 1.54184 Å
Cell parameters from 24601 reflections
θ = 3.9–76.3°
μ = 10.25 mm^{-1}
T = 100 K
Prism, colourless
0.12 × 0.11 × 0.08 mm

Data collection

Rigaku XtaLAB Synergy Dualflex AtlasS2 diffractometer
Detector resolution: 5.2558 pixels mm^{-1}
ω scans
Absorption correction: gaussian (CrysAlis PRO; Rigaku OD, 2018)
T_{min} = 0.840, T_{max} = 1.000
28219 measured reflections
4248 independent reflections
4231 reflections with $I > 2\sigma(I)$
R_{int} = 0.022
θ_{max} = 67.1°, θ_{min} = 3.9°
h = −11→11
k = −13→13
l = −13→14

Refinement

Refinement on F^2
Least-squares matrix: full
$R[F^2 > 2\sigma(F^2)]$ = 0.015
$wR(F^2)$ = 0.040
S = 1.00
4248 reflections
266 parameters
0 restraints
Primary atom site location: structure-invariant direct methods
Secondary atom site location: difference Fourier map
Hydrogen site location: inferred from neighbouring sites
H-atom parameters constrained

$w = 1/[\sigma^2(F_o^2) + (0.026P)^2 + 0.5977P]$
where $P = (F_o^2 + 2F_c^2)/3$
$(\Delta/\sigma)_{max} = 0.001$

$\Delta\rho_{max} = 0.36$ e Å^{-3}
$\Delta\rho_{min} = -0.44$ e Å^{-3}

Special details

Geometry. All esds (except the esd in the dihedral angle between two l.s. planes) are estimated using the full covariance matrix. The cell esds are taken into account individually in the estimation of esds in distances, angles and torsion angles; correlations between esds in cell parameters are only used when they are defined by crystal symmetry. An approximate (isotropic) treatment of cell esds is used for estimating esds involving l.s. planes.

Fractional atomic coordinates and isotropic or equivalent isotropic displacement parameters (Å²)

	x	*y*	*z*	U_{iso}*/U_{eq}
Sn	0.39008 (2)	0.31848 (2)	0.21713 (2)	0.01326 (4)
S1	0.19166 (4)	0.50402 (3)	0.11108 (3)	0.01639 (8)
S2	0.17439 (4)	0.47895 (4)	0.36811 (3)	0.01880 (8)
N1	−0.00996 (14)	0.67737 (12)	0.22420 (12)	0.0176 (3)
C1	0.10482 (15)	0.56682 (14)	0.23615 (14)	0.0157 (3)
C2	−0.08409 (18)	0.72965 (17)	0.33124 (16)	0.0259 (4)
H2	−0.0355	0.6655	0.4017	0.031*
C3	−0.24831 (19)	0.74782 (18)	0.34878 (17)	0.0301 (4)
H3A	−0.3009	0.8147	0.2840	0.045*
H3B	−0.2902	0.7723	0.4243	0.045*
H3C	−0.2600	0.6682	0.3493	0.045*
C4	−0.0574 (2)	0.8507 (2)	0.3257 (2)	0.0454 (5)
H4A	0.0498	0.8342	0.3141	0.068*
H4B	−0.0976	0.8788	0.3998	0.068*
H4C	−0.1073	0.9170	0.2594	0.068*
C5	−0.07259 (17)	0.75964 (14)	0.11003 (14)	0.0196 (3)
H5	−0.1546	0.8354	0.1323	0.023*
C6	−0.1481 (2)	0.69886 (17)	0.05404 (17)	0.0273 (4)
H6A	−0.2025	0.7616	−0.0122	0.041*
H6B	−0.2180	0.6691	0.1132	0.041*
H6C	−0.0727	0.6267	0.0250	0.041*
C7	0.03571 (19)	0.81240 (16)	0.02586 (16)	0.0278 (4)
H7A	0.1147	0.7437	−0.0056	0.042*
H7B	0.0798	0.8497	0.0683	0.042*
H7C	−0.0173	0.8779	−0.0396	0.042*
C11	0.55885 (16)	0.34926 (13)	0.28704 (13)	0.0147 (3)
C12	0.68313 (16)	0.35637 (15)	0.21077 (14)	0.0191 (3)
H12	0.6918	0.3435	0.1331	0.023*
C13	0.79426 (17)	0.38199 (16)	0.24707 (15)	0.0228 (3)
H13	0.8761	0.3902	0.1931	0.027*
C14	0.78624 (17)	0.39561 (15)	0.36188 (16)	0.0220 (3)
H14	0.8633	0.4115	0.3872	0.026*
C15	0.66454 (17)	0.38591 (14)	0.43962 (15)	0.0195 (3)
H15	0.6594	0.3934	0.5188	0.023*
C16	0.55062 (16)	0.36527 (14)	0.40185 (14)	0.0167 (3)
H16	0.4661	0.3620	0.4546	0.020*

C21	0.31244 (16)	0.16861 (14)	0.31013 (13)	0.0161 (3)
C22	0.40747 (18)	0.05244 (15)	0.37020 (15)	0.0215 (3)
H22	0.5088	0.0403	0.3739	0.026*
C23	0.3558 (2)	−0.04562 (16)	0.42466 (16)	0.0256 (4)
H23	0.4216	−0.1239	0.4661	0.031*
C24	0.20910 (19)	−0.03021 (16)	0.41896 (15)	0.0227 (3)
H24	0.1740	−0.0975	0.4565	0.027*
C25	0.11378 (18)	0.08408 (17)	0.35814 (16)	0.0255 (4)
H25	0.0132	0.0950	0.3529	0.031*
C26	0.16529 (18)	0.18255 (16)	0.30497 (15)	0.0234 (3)
H26	0.0989	0.2610	0.2643	0.028*
C31	0.50078 (15)	0.25703 (14)	0.05537 (14)	0.0162 (3)
C32	0.55917 (18)	0.12811 (15)	0.05353 (16)	0.0229 (3)
H32	0.5551	0.0668	0.1246	0.027*
C33	0.62313 (19)	0.08811 (16)	−0.05083 (17)	0.0282 (4)
H33	0.6622	0.0000	−0.0505	0.034*
C34	0.63013 (19)	0.17592 (18)	−0.15492 (16)	0.0272 (4)
H34	0.6732	0.1483	−0.2262	0.033*
C35	0.57407 (19)	0.30455 (17)	−0.15524 (15)	0.0249 (3)
H35	0.5790	0.3653	−0.2265	0.030*
C36	0.51064 (17)	0.34382 (15)	−0.05060 (14)	0.0197 (3)
H36	0.4731	0.4319	−0.0512	0.024*

Atomic displacement parameters (Å²)

	U^{11}	U^{22}	U^{33}	U^{12}	U^{13}	U^{23}
Sn	0.01301 (6)	0.01352 (6)	0.01339 (6)	−0.00463 (4)	−0.00068 (4)	−0.00360 (4)
S1	0.01698 (17)	0.01653 (17)	0.01422 (18)	−0.00254 (13)	−0.00113 (13)	−0.00638 (13)
S2	0.01615 (17)	0.02318 (18)	0.01490 (18)	−0.00338 (14)	−0.00031 (13)	−0.00680 (14)
N1	0.0147 (6)	0.0194 (6)	0.0190 (7)	−0.0035 (5)	−0.0015 (5)	−0.0083 (5)
C1	0.0122 (6)	0.0189 (7)	0.0187 (8)	−0.0070 (6)	0.0006 (5)	−0.0076 (6)
C2	0.0201 (8)	0.0305 (9)	0.0226 (9)	0.0009 (7)	0.0008 (6)	−0.0153 (7)
C3	0.0253 (9)	0.0306 (9)	0.0286 (10)	−0.0063 (7)	0.0080 (7)	−0.0087 (7)
C4	0.0423 (11)	0.0616 (14)	0.0523 (14)	−0.0251 (10)	0.0112 (10)	−0.0445 (12)
C5	0.0184 (7)	0.0170 (7)	0.0221 (8)	−0.0032 (6)	−0.0043 (6)	−0.0053 (6)
C6	0.0278 (9)	0.0265 (9)	0.0297 (10)	−0.0086 (7)	−0.0116 (7)	−0.0057 (7)
C7	0.0280 (9)	0.0232 (8)	0.0295 (10)	−0.0081 (7)	0.0028 (7)	−0.0061 (7)
C11	0.0136 (6)	0.0116 (6)	0.0173 (8)	−0.0025 (5)	−0.0032 (5)	−0.0026 (5)
C12	0.0153 (7)	0.0211 (7)	0.0178 (8)	−0.0027 (6)	−0.0015 (6)	−0.0048 (6)
C13	0.0134 (7)	0.0265 (8)	0.0256 (9)	−0.0058 (6)	0.0005 (6)	−0.0045 (7)
C14	0.0154 (7)	0.0208 (8)	0.0312 (9)	−0.0049 (6)	−0.0071 (6)	−0.0068 (7)
C15	0.0217 (7)	0.0157 (7)	0.0200 (8)	−0.0025 (6)	−0.0053 (6)	−0.0065 (6)
C16	0.0159 (7)	0.0142 (7)	0.0178 (8)	−0.0031 (5)	−0.0009 (6)	−0.0038 (6)
C21	0.0192 (7)	0.0169 (7)	0.0139 (7)	−0.0078 (6)	0.0014 (6)	−0.0058 (6)
C22	0.0210 (8)	0.0211 (8)	0.0230 (8)	−0.0084 (6)	−0.0041 (6)	−0.0029 (6)
C23	0.0315 (9)	0.0184 (8)	0.0249 (9)	−0.0081 (7)	−0.0041 (7)	−0.0019 (7)
C24	0.0314 (9)	0.0233 (8)	0.0192 (8)	−0.0168 (7)	0.0075 (6)	−0.0094 (6)
C25	0.0204 (8)	0.0312 (9)	0.0291 (9)	−0.0140 (7)	0.0047 (7)	−0.0104 (7)

C26	0.0182 (8)	0.0229 (8)	0.0264 (9)	−0.0060 (6)	−0.0006 (6)	−0.0036 (7)
C31	0.0131 (7)	0.0189 (7)	0.0179 (8)	−0.0054 (6)	−0.0003 (5)	−0.0071 (6)
C32	0.0225 (8)	0.0194 (8)	0.0260 (9)	−0.0062 (6)	0.0008 (6)	−0.0074 (7)
C33	0.0265 (8)	0.0225 (8)	0.0389 (10)	−0.0074 (7)	0.0034 (7)	−0.0180 (8)
C34	0.0241 (8)	0.0378 (10)	0.0267 (9)	−0.0127 (7)	0.0062 (7)	−0.0212 (8)
C35	0.0270 (8)	0.0312 (9)	0.0189 (8)	−0.0134 (7)	0.0027 (6)	−0.0079 (7)
C36	0.0201 (7)	0.0201 (8)	0.0201 (8)	−0.0071 (6)	0.0001 (6)	−0.0078 (6)

Geometric parameters (Å, º)

Sn—S1	2.4792 (4)	C12—H12	0.9500
Sn—S2	2.9264 (4)	C13—C14	1.387 (3)
Sn—C11	2.1446 (14)	C13—H13	0.9500
Sn—C21	2.1349 (15)	C14—C15	1.391 (2)
Sn—C31	2.1754 (15)	C14—H14	0.9500
C1—S1	1.7587 (15)	C15—C16	1.388 (2)
C1—S2	1.7006 (16)	C15—H15	0.9500
C1—N1	1.336 (2)	C16—H16	0.9500
C5—N1	1.495 (2)	C21—C26	1.391 (2)
C2—N1	1.497 (2)	C21—C22	1.394 (2)
C2—C3	1.517 (2)	C22—C23	1.387 (2)
C2—C4	1.519 (3)	C22—H22	0.9500
C2—H2	1.0000	C23—C24	1.383 (2)
C3—H3A	0.9800	C23—H23	0.9500
C3—H3B	0.9800	C24—C25	1.385 (3)
C3—H3C	0.9800	C24—H24	0.9500
C4—H4A	0.9800	C25—C26	1.387 (2)
C4—H4B	0.9800	C25—H25	0.9500
C4—H4C	0.9800	C26—H26	0.9500
C5—C7	1.515 (2)	C31—C32	1.397 (2)
C5—C6	1.519 (2)	C31—C36	1.396 (2)
C5—H5	1.0000	C32—C33	1.391 (3)
C6—H6A	0.9800	C32—H32	0.9500
C6—H6B	0.9800	C33—C34	1.382 (3)
C6—H6C	0.9800	C33—H33	0.9500
C7—H7A	0.9800	C34—C35	1.388 (3)
C7—H7B	0.9800	C34—H34	0.9500
C7—H7C	0.9800	C35—C36	1.390 (2)
C11—C12	1.395 (2)	C35—H35	0.9500
C11—C16	1.397 (2)	C36—H36	0.9500
C12—C13	1.388 (2)		

C21—Sn—C11	119.87 (6)	C12—C11—C16	118.47 (14)
C21—Sn—C31	102.73 (6)	C12—C11—Sn	117.04 (11)
C11—Sn—C31	103.38 (5)	C16—C11—Sn	124.47 (11)
C21—Sn—S1	112.27 (4)	C13—C12—C11	120.79 (15)
C11—Sn—S1	119.12 (4)	C13—C12—H12	119.6
C31—Sn—S1	93.24 (4)	C11—C12—H12	119.6

C21—Sn—S2	88.10 (4)	C14—C13—C12	120.24 (15)
C11—Sn—S2	86.68 (4)	C14—C13—H13	119.9
C31—Sn—S2	158.41 (4)	C12—C13—H13	119.9
S1—Sn—S2	65.260 (11)	C13—C14—C15	119.49 (15)
C1—S1—Sn	95.87 (5)	C13—C14—H14	120.3
C1—S2—Sn	82.36 (5)	C15—C14—H14	120.3
C1—N1—C5	125.74 (13)	C14—C15—C16	120.21 (15)
C1—N1—C2	119.61 (13)	C14—C15—H15	119.9
C5—N1—C2	114.62 (12)	C16—C15—H15	119.9
N1—C1—S2	123.73 (12)	C15—C16—C11	120.71 (14)
N1—C1—S1	119.94 (12)	C15—C16—H16	119.6
S2—C1—S1	116.33 (8)	C11—C16—H16	119.6
N1—C2—C3	111.83 (14)	C26—C21—C22	118.14 (14)
N1—C2—C4	110.44 (15)	C26—C21—Sn	119.77 (11)
C3—C2—C4	112.51 (15)	C22—C21—Sn	121.95 (11)
N1—C2—H2	107.3	C23—C22—C21	120.74 (15)
C3—C2—H2	107.3	C23—C22—H22	119.6
C4—C2—H2	107.3	C21—C22—H22	119.6
C2—C3—H3A	109.5	C24—C23—C22	120.43 (15)
C2—C3—H3B	109.5	C24—C23—H23	119.8
H3A—C3—H3B	109.5	C22—C23—H23	119.8
C2—C3—H3C	109.5	C23—C24—C25	119.52 (15)
H3A—C3—H3C	109.5	C23—C24—H24	120.2
H3B—C3—H3C	109.5	C25—C24—H24	120.2
C2—C4—H4A	109.5	C24—C25—C26	119.94 (15)
C2—C4—H4B	109.5	C24—C25—H25	120.0
H4A—C4—H4B	109.5	C26—C25—H25	120.0
C2—C4—H4C	109.5	C21—C26—C25	121.22 (15)
H4A—C4—H4C	109.5	C21—C26—H26	119.4
H4B—C4—H4C	109.5	C25—C26—H26	119.4
N1—C5—C7	113.59 (13)	C32—C31—C36	117.70 (14)
N1—C5—C6	112.50 (13)	C32—C31—Sn	120.43 (12)
C7—C5—C6	114.30 (15)	C36—C31—Sn	121.81 (11)
N1—C5—H5	105.1	C33—C32—C31	120.96 (16)
C7—C5—H5	105.1	C33—C32—H32	119.5
C6—C5—H5	105.1	C31—C32—H32	119.5
C5—C6—H6A	109.5	C34—C33—C32	120.27 (16)
C5—C6—H6B	109.5	C34—C33—H33	119.9
H6A—C6—H6B	109.5	C32—C33—H33	119.9
C5—C6—H6C	109.5	C33—C34—C35	119.89 (16)
H6A—C6—H6C	109.5	C33—C34—H34	120.1
H6B—C6—H6C	109.5	C35—C34—H34	120.1
C5—C7—H7A	109.5	C36—C35—C34	119.53 (16)
C5—C7—H7B	109.5	C36—C35—H35	120.2
H7A—C7—H7B	109.5	C34—C35—H35	120.2
C5—C7—H7C	109.5	C35—C36—C31	121.64 (15)
H7A—C7—H7C	109.5	C35—C36—H36	119.2
H7B—C7—H7C	109.5	C31—C36—H36	119.2

C5—N1—C1—S2	178.33 (11)	C13—C14—C15—C16	−1.3 (2)
C2—N1—C1—S2	0.0 (2)	C14—C15—C16—C11	2.4 (2)
C5—N1—C1—S1	−2.2 (2)	C12—C11—C16—C15	−0.9 (2)
C2—N1—C1—S1	179.49 (11)	Sn—C11—C16—C15	−179.42 (11)
Sn—S2—C1—N1	−176.75 (13)	C26—C21—C22—C23	−0.9 (2)
Sn—S2—C1—S1	3.78 (7)	Sn—C21—C22—C23	−176.59 (13)
Sn—S1—C1—N1	176.06 (11)	C21—C22—C23—C24	0.8 (3)
Sn—S1—C1—S2	−4.44 (8)	C22—C23—C24—C25	0.1 (3)
C1—N1—C2—C3	−120.82 (16)	C23—C24—C25—C26	−0.9 (3)
C5—N1—C2—C3	60.70 (19)	C22—C21—C26—C25	0.1 (2)
C1—N1—C2—C4	113.06 (18)	Sn—C21—C26—C25	175.91 (13)
C5—N1—C2—C4	−65.42 (18)	C24—C25—C26—C21	0.8 (3)
C1—N1—C5—C7	−64.0 (2)	C36—C31—C32—C33	−0.8 (2)
C2—N1—C5—C7	114.38 (15)	Sn—C31—C32—C33	176.56 (12)
C1—N1—C5—C6	67.84 (19)	C31—C32—C33—C34	0.1 (3)
C2—N1—C5—C6	−113.79 (15)	C32—C33—C34—C35	0.5 (3)
C16—C11—C12—C13	−1.6 (2)	C33—C34—C35—C36	−0.3 (3)
Sn—C11—C12—C13	176.97 (12)	C34—C35—C36—C31	−0.4 (2)
C11—C12—C13—C14	2.7 (2)	C32—C31—C36—C35	1.0 (2)
C12—C13—C14—C15	−1.3 (2)	Sn—C31—C36—C35	−176.35 (12)

Hydrogen-bond geometry (Å, º)

D—H···*A*	*D*—H	H···*A*	*D*···*A*	*D*—H···*A*
C34—H34···C24^{i}	0.95	2.82	3.757 (3)	171

Symmetry code: (i) −*x*+1, −*y*, −*z*.